Doppler Radar and Lightning Network Observations of a Severe Outbreak of Tropical Cyclone Tornadoes

EUGENE W. MCCAUL JR.

Universities Space Research Association, Huntsville, Alabama

DENNIS E. BUECHLER

University of Alabama in Huntsville, Huntsville, Alabama

STEVEN J. GOODMAN

NASA Marshall Space Flight Center, Huntsville, Alabama

MICHAEL CAMMARATA

National Weather Service, Columbia, South Carolina

(Manuscript received 7 August 2003, in final form 15 December 2003)

ABSTRACT

Data from a single Weather Surveillance Radar-1988 Doppler (WSR-88D) and the National Lightning Detection Network are used to examine the characteristics of the convective storms that produced a severe tornado outbreak, including three tornadoes that reached F3 intensity, within Tropical Storm Beryl's remnants on 16 August 1994. Comparison of the radar data with reports of tornadoes suggests that only 13 cells produced the 29 tornadoes that were documented in Georgia and the Carolinas on that date. Six of these cells spawned multiple tornadoes, and the radar data confirm the presence of miniature supercells. One of the cells was identifiable on radar for 11 h, spawning tornadoes over a time period spanning approximately 6.5 h. Several other tornadic cells also exhibited great longevity, with cell lifetimes longer than ever previously documented in a landfalling tropical cyclone (TC) tornado event. This event is easily the most intense TC tornado outbreak yet documented with WSR-88Ds.

Time–height analyses of the three strongest tornadic supercells are presented in order to document storm kinematic structure and to show how these storms appear at different ranges from a WSR-88D. In addition, cloud-to-ground (CG) lightning data are examined in Beryl's remnants. Although the tornadic cells were responsible for most of Beryl's CG lightning, their flash rates were only weak to moderate, and in all the tornadic storms the lightning flashes were almost entirely negative in polarity. A few of the single-tornado storms produced no detectable CG lightning at all. There is evidence that CG lightning rates decreased during the tornadoes, compared to 30-min periods before the tornadoes. A number of the storms spawned tornadoes just after producing their final CG lightning flashes. Contrary to the findings for flash rates, both peak currents and positive flash percentages were larger in Beryl's nontornadic storms than in the tornadic ones.

1. Introduction

It is well known that most tropical cyclones (TCs) that make landfall along the Gulf Coast of the United States spawn at least a few tornadoes (McCaul 1991). Although most landfalling TCs generate fewer than a dozen such tornadoes, a small proportion produce large swarm outbreaks, with as many as 30 or more tornadoes. Study of the statistical distribution of the numbers of tornadoes spawned by TCs led McCaul (1991) to define a ''severe'' TC tornado outbreak as one consisting of at least 24 tornadoes. Usually, these severe outbreaks occur in large, intense hurricane-strength TCs (Novlan and Gray 1974; McCaul 1991), but on 15–17 August 1994 Tropical Storm (TS) Beryl generated 37 tornadoes along its path from the Florida panhandle through the mid-Atlantic states. Some 32 of these tornadoes occurred on 16 August 1994 alone from eastern Georgia to southern Virginia, with most of these taking place in South Carolina; 29 of these tornadoes occurred during the period encompassed by this study.

The Beryl outbreak is especially noteworthy in that at least three of the tornadoes achieved peak intensity

Corresponding author address: Eugene W. McCaul Jr., Universities Space Research Association, 6700 Odyssey Drive, Suite 203, Huntsville, AL 35806.
E-mail: mccaul@space.hsv.usra.edu

of F3 on the Fujita (1981) damage intensity scale. Although no fatalities resulted from the Beryl outbreak, at least 50 persons suffered injuries, and property damages totaled more than $50 million (Vescio et al. 1996). Tropical Storm Beryl is a good example of a TC whose greatest danger to the public is its postlandfall severe weather. In this respect, and in the character of its swarm outbreak of tornadoes, it resembles another large tornado outbreak spawned by a relatively weak TC, Hurricane Danny of 1985 (McCaul 1987). In the Danny outbreak, numerous minisupercell storms were found to have occurred, and it was noted that, because of the storms' relatively shallow depth, cloud-to-ground (CG) lightning rates were very small. Better observations of future TC tornado outbreaks, especially with modern surveillance tools such as Doppler radars and lightning detection and mapping equipment, were recommended. This study attempts to follow up on those recommendations.

Although the Beryl tornado outbreak is not the first set of TC-spawned tornadic storms to be observed with the national network of WSR-88D units, it is the most intense such outbreak. As of this writing, Beryl's 37 total tornadoes rank it in sixth place historically in terms of U.S. TC tornado productivity. In addition, only two other landfalling TCs have spawned more F3–F4 tornadoes than Beryl: Carla of 1961 with eight and Beulah of 1967 with six. Ten of the 29 tornadoes studied here were rated F2 or stronger, yielding a significant tornado fraction of 0.34. This is slightly larger than the 0.31 fraction found in Hurricane Danny of 1985, and also larger than the overall average of 0.26 for all the TC-spawned tornadoes in the 1948–86 database of McCaul (1991). Although some 21 tornadoes occurred in Florida in conjunction with the Tropical Storm Josephine outbreak of 1996 studied by Spratt et al. (1998), only one tornado was found to be F2, for a significant tornado fraction of only 0.05. The corresponding significant tornado fraction for the United States–wide 1950–76 tornado database studied by Kelly et al. (1978) was 0.36.

The purposes of this paper are to document the radar-derived characteristics of Beryl's tornadic storms to see how they compare in general with earlier observations (McCaul 1987) and numerical simulations of such storms (McCaul and Weisman 1996a) and to examine the CG lightning activity in Beryl's storms in an attempt to find patterns that might help anticipate severe weather. One question of particular interest is whether or not the storms assumed the form of minisupercells (see McCaul 1987; Davies 1990, 1993; McCaul and Weisman 1996a). Such supercells, because of the characteristics of the environments in which they form (see McCaul and Weisman 1996a), tend to have modal echo tops near 10 km or less, instead of the 15 km or so seen in large, midlatitude supercells. They also have somewhat narrower updrafts, mesocyclones, and reflectivity echo footprints and are thus more difficult to recognize as being potentially severe, especially at longer ranges from radars. Their smaller depth also limits the quantity of mixed-phase hydrometeors aloft in regions favorable for charge separation, leading to reduced lightning rates, which further impedes the ability of the public to recognize the storms as being potentially dangerous.

We begin by using composite mosaic radar reflectivity images to examine the overall spatial distribution of the tornado outbreak and to identify which cells produced tornadoes. We then use WSR-88D data to study the characteristics of some of the tornadic cells. Although we have velocity data from only a single WSR-88D, we are able to use these data to study how the tornadic mesocyclone signatures look at various ranges from the radar, to see how mesocyclone rotation rates relate to surface tornado reports, and to see how mesocyclone vertical structure varies with time. We also examine the WSR-88D-derived mesoscale wind profiles as a function of time to see whether any localized increases in vertical shear accompany the tornado activity. In addition, we also study CG lightning data collected by the National Lightning Detection Network (NLDN; Cummins et al. 1998) to document the CG flash rates, polarities, and peak currents in Beryl's tornadic and nontornadic convection and to document how the CG rates vary with time as the tornadic cells evolve. Using NLDN data, we are able to document the CG lightning activity throughout all of Beryl's remnants.

Section 2 presents a summary of the data and analysis techniques employed in this study. Section 3 contains a description of the general statistics of the Beryl tornado outbreak and its attendant meteorological conditions, along with the results of our analyses of the WSR-88D and NLDN data. In section 4, we give a contextual discussion of the results of section 3. We summarize our findings and make suggestions for future work in section 5.

2. Data analysis

The kinematic and thermodynamic environment supporting Beryl's tornadic convection was examined using both surface and upper-air data, along with wind profile products from a National Weather Service (NWS) Doppler radar in the vicinity of the tornadoes. The characteristics of the tornadic storms themselves were studied with regional radar mosaic imagery and single-Doppler radar data, along with lightning strike data from NLDN.

To determine which storm cells were responsible for the tornadoes, we inspected WSI Corporation's NOWrad regional 15-min radar reflectivity mosaic images from 1200 UTC 16 August to 0300 UTC 17 August 1994 and located the 29 tornadoes reported in *Storm Data* (NCDC 1994) within these radar images. With few exceptions, it was possible to identify readily which echoes were responsible for the tornadoes. Using this method, we identified 13 separate tornadic cells that spawned the 29 tornadoes. We also

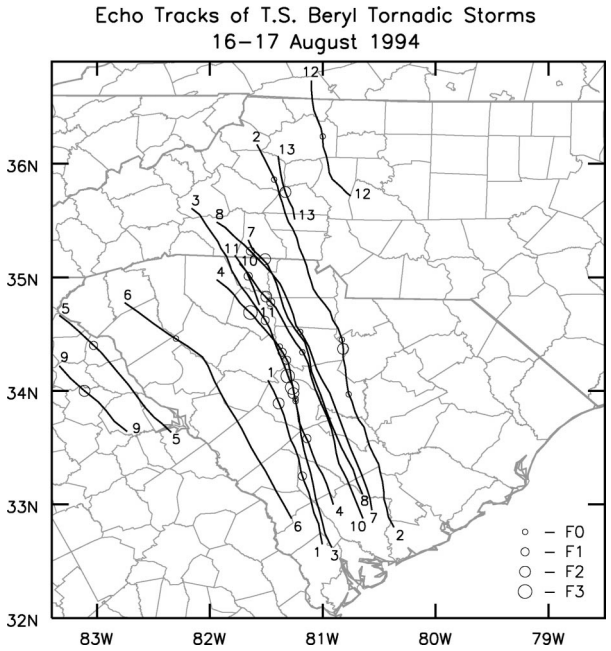

FIG. 1. Locations of the smoothed echo centroid tracks for the 13 tornado-producing storms spawned by TS Beryl in Georgia and the Carolinas on 16–17 Aug 1994. Storm identification (ID) numbers are the same as those listed in Table 2. Circles marked along each echo centroid track indicate cell locations at start times of the tornadoes reported in *Storm Data* (NCDC 1994). Diameters of the circles correspond to the observed Fujita scale estimates, as per the legend provided at lower right. Actual tornado locations, not shown for clarity, were generally near or several km to the east of the circles.

documented the approximate times of cell genesis and decay, and characteristic cell motion vectors for each cell. The tracks of these tornadic cells are depicted in Fig. 1, and the 29 tornadoes associated with these storm cells are cataloged in Table 1.

One of the tornadoes (number 15 in Table 1) was listed as occurring at a time and place that did not correspond to any significant radar echo. In this case, we assumed that the time of the tornado was in error due to delayed reporting and searched backward in time for the next prior convective cell that passed over the location of the reported tornado. The cell so identified happened to be a known long-lived tornadic cell (storm 2) and thus a likely candidate for the storm that actually produced the tornado. Accordingly, in Table 1 we have modified the start and end times of this tornado to correspond to the time period when storm 2's mesocyclone passed over the tornado location.

Once all the tornadic cells were identified and cataloged, we proceeded to study individual cell characteristics using available NWS Doppler radar data. The WSR-88D at Columbia, South Carolina (KCAE), was convenient for this purpose because it was located close to the center of Beryl's tornado activity. Many of the tornadic storms passed within 30 km of the radar, and at least one tornado was sighted visually from the collocated NWS office. A relatively complete archive of level 4 graphical data, including reflectivity and velocity scans, velocity–azimuth display (VAD) products, vertically integrated liquid (VIL), and echo-top data, was written at KCAE for the Beryl tornado outbreak. Level 2 data were not recorded.

In Fig. 2 are depicted regional views of the mosaic radar reflectivity fields at 1600, 1800, 2000, and 2200 UTC 16 August 1994. These times include the peak of the tornado outbreak and reveal how the tornadic cells were arranged within the overall precipitation shield structure of TS Beryl, which was centered over southwestern Georgia at 1600 UTC, moving northeast. From Figs. 1 and 2, it is clear that most of the tornadic cells occurred in the right-front or northeast quadrant of Beryl. This location is consistent with what is observed in most tropical cyclone tornado outbreaks (Novlan and Gray 1974; McCaul 1991).

As it happens, three of the strongest tornadic cells, storms 2, 3, and 4, passed within 30 km of KCAE and produced tornadoes for many hours. KCAE was able to observe these cells while they produced tornadoes at ranges as small as 10 km and as great as 147 km from KCAE. Although these storms were not perfectly steady state in terms of structure during this period of study, they continued to produce tornadoes, making the temporal evolution of their radar signatures a subject of interest.

To document the structure of storms 2–4 as seen on radar at these varying ranges, we performed complete time–height analyses of them for the period 1500 to 2148 UTC, the latter time corresponding to the time the last cell exited the unambiguous velocity range of KCAE, approximately 147 km north of the radar. Radar parameters documented in this analysis included storm-relative mesocyclone rotational velocity (V_R), rotational shear vorticity (ζ), and mesocyclone diameter (ϕ; measured across the couplet of strongest inbound and outbound velocities), as a function of range, elevation angle, and altitude. Time series of WSR-88D estimated 30-dBZ echo-top heights (z_T) and VIL were also recorded for each cell. Because radar data were available only in level 4 format, point values of velocity, VIL, and z_T were assigned using midrange values of the contoured graphical data. Rotational shear vorticity was evaluated using twice V_R divided by half the diameter ϕ. Using the measured V_R and ϕ data, we also constructed profiles of mesocyclone angular momentum per unit mass $(1/2)\phi V_R$. In addition to these cell-specific analyses, the evolution of the larger mesoscale wind profiles was studied by examining the time series of velocity–azimuth display winds obtained by KCAE, in conjunction with inspection of patterns in hourly surface wind observations.

Portions of the KCAE radar data must be studied with caution. Two of the tornadic mesocyclones (those from storms 3 and 4) passed well within the KCAE cone of silence, at ranges as close as 10 km. During these periods, velocity data sometimes became contaminated

TABLE 1. Tornadoes in KCAE WSR-88D region during TS Beryl outbreak, 1500 UTC 16 Aug–0015 UTC 17 Aug 1994. N: tornado number; UTC1 (UTC2): starting (ending) time of tornado; Start (End) loc: starting (ending) location of tornado, known or estimated from information in *Storm Data* (NCDC 1994); ST: state abbreviation for the starting or ending location; F: F-scale rating of tornado; PW: tornado path width (yd); PL: tornado path length (mi); STM: tornado parent storm cell ID number (see Fig. 1).

N	UTC1	UTC2	Start loc (miles)	ST	End loc (miles)	ST	F	PW	PL	STM
1	1509	1530	Govan 5 SSE	SC	Govan 1 N	SC	1	75	5.00	1
2	1620	1625	Neeses	SC	Neeses	SC	1	50	0.07	4
3	1700	1702	Gilbert 3 SE	SC	Gilbert 3 SE	SC	2	50	0.06	1
4	1716	1716	Edmund SE	SC	Edmund N	SC	0	30	0.50	4
5	1727	1730	Lexington 5 S	SC	Red Bank	SC	2	25	2.00	4
6	1730	1737	MMT 1 SSE	SC	MMT arpt 1 NNE	SC	0	50	2.00	2
7	1735	1750	Lexington 3 SSE	SC	Lake Murray	SC	3	440	8.00	4
8	1739	1741	Hartwell 4 S	GA	Hartwell 3 SW	GA	1	100	1.00	5
9	1753	1810	KCAE 3 SW	SC	KCAE 3 SW	SC	0	100	0.10	3
10	1815	1817	Lexington 5 N	GA	Lexington 6 NNW	GA	2	200	1.00	9
11	1818	1822	Ballentine 1 N	SC	Ballentine 2 NNW	SC	1	75	1.00	4
12	1832	1834	Peak	SC	Peak	SC	1	50	0.50	4
13	1835	1837	Lexington 4 S	SC	Lexington 4 S	SC	3	75	0.30	3
14	1843	1845	Strother	SC	Dawkins	SC	0	50	0.50	4
15	1846	1849	Ridgeway 9 NE	SC	Ridgeway 9 NE	SC	2	50	0.30	2
16	1900	1902	Liberty Hill	SC	Liberty Hill	SC	0	50	0.08	2
17	1940	1940	Ware Shoals	SC	Ware Shoals	SC	0	30	0.10	6
18	1950	2100	Santuc	SC	Cowpens 2 S	SC	3	250	30.00	4
19	2000	2122	Carlisle	SC	Cowpens 2 S	SC	1	150	30.00	3
20	2144	2146	Winnsboro 8 SSW	SC	Winnsboro 8 SSW	SC	0	100	0.06	10
21	2150	2152	York 4 S	SC	York 4 S	SC	0	50	0.08	7
22	2156	2202	Cowpens 6 E	SC	Cowpens 5 NE	SC	1	75	3.00	11
23	2230	2234	Earl	NC	Earl 2 NW	NC	1	200	2.00	8
24	2236	2245	Blacksburg	SC	Blacksburg 4 NNW	NC	2	100	4.00	7
25	2255	2258	Chester 7 W	SC	Chester 7 W	SC	1	75	0.25	10
26	2305	2320	Lockhart	SC	Lockhart 10 NW	SC	2	150	10.00	10
27	2342	0002	Dudley Shoals	NC	Kings Creek	NC	0	unk	10.00	2
28	2345	2348	Hickory NE	NC	Hickory NNE	NC	2	200	1.50	13
29	0015	0015	Lomax	NC	Sheppards Crossroads	NC	0	unk	unk	12

with ground clutter, and VIL and z_T data became unreliable because of incomplete volume sampling of the storms. In addition, a power failure at KCAE, apparently caused by nearby tornado damage, led to a loss of all radar data from 1722 to 1739 UTC.

We also examined CG lightning data from NLDN for the tornadic storms in the Beryl outbreak. In this part of the study, we identified CG flashes as a function of time for each tornadic cell. The CG lightning was assigned to the individual tornadic cells by plotting flash locations at 15-min intervals on each WSI radar mosaic image, then associating clusters of flashes with radar echoes that were approximately collocated. Flash information such as time, location, polarity, peak current, and stroke multiplicity were then tabulated for these cell-related CG flash clusters, using a 5-min time discretization, as in other NLDN tornadic storm studies (e.g., MacGorman 1993). This 5-min time discretization is also approximately the same as that for the KCAE WSR-88D radar volume scans, but for radar-based data plots presented later, CG flash counts pertinent to the actual radar scan time intervals are displayed. While these procedures allowed us to document CG flash data for the tornadic cells, we were also able to use the NLDN data to document all the CG lightning in Beryl's remnants during the tornado outbreak study period, even for the nontornadic convection. However, we did not attempt to count nontornadic cells or assign CG flash counts to them on an individual basis.

Because NLDN data are available over the entire United States, our analyses of the CG flash data represent all Beryl's convective cells with a nearly uniform spatial coverage. Although we were able to track the lifetimes of all the tornadic cells with comparable thoroughness using the mosaic radar composite images, a correspondingly thorough Doppler velocity analysis of all 13 tornadic storms was not feasible, owing to the inherent limitations of the radar surveillance coverage and the magnitude of the radar analysis task. Likewise, we were not able to perform radar analyses of all the nontornadic cells of 16 August to see whether they contained Doppler-derived mesocyclone signatures and, if present, how they differed from those of the tornadic storms. The latter information might be potentially useful for minimization of the false alarm rate in automated mesocyclone detection algorithms. Suzuki et al. (2000) found that only three of nine supercells observed within a Japanese typhoon produced tornadoes, a ratio which, if found to be representative in the United States, suggests the false alarm problem is significant.

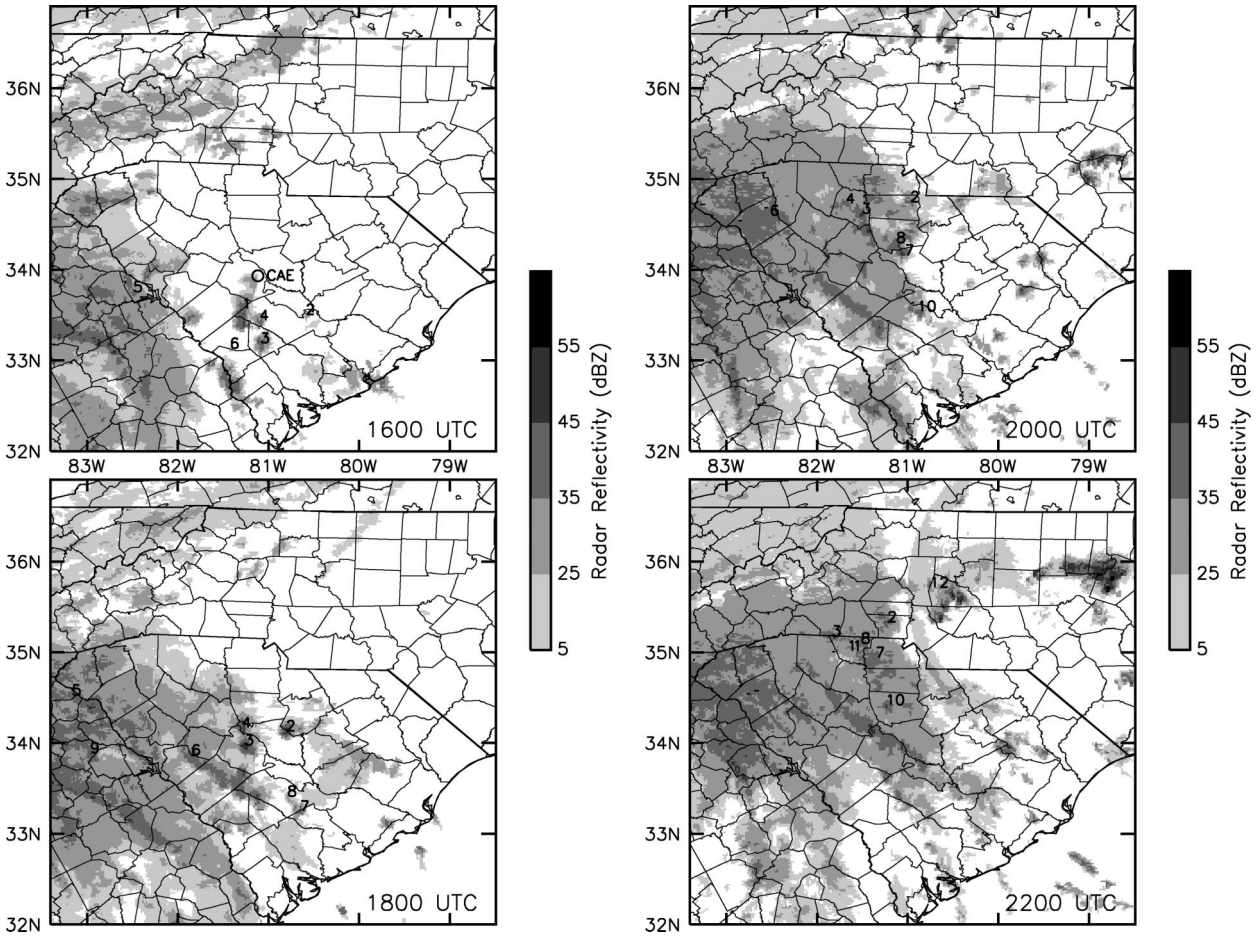

FIG. 2. Regional-scale mosaic reflectivity fields at 1600, 1800, 2000, and 2200 UTC 16 Aug 1994, during the TS Beryl tornado outbreak. Tornadic storm cells are labeled on their eastern or northeastern flanks with numbers assigned in Table 2. The location of the Columbia radar (KCAE) is shown with a circle in the 1600 UTC panel.

3. Results

a. Outbreak statistics

The tornado productivity and echo and lightning histories of the 13 identified tornadic cells are summarized in Table 2. For each cell, the table includes the times of first and last echo, times of first and last tornadoes, intensity rating of the cell's strongest tornado, times of first and last CG lightning flashes and total numbers of flashes of positive and negative polarity.

Table 2 shows that 6 of the 13 cells were multiple tornado producers. Storms 2, 3, and 4 accounted for 15 of the 29 tornadoes studied in this paper, with storm 4 spawning 8 of these. Storms 3 and 4 both produced F3 intensity tornadoes. Although storm 2 produced four tornadoes, the strongest being F2 in intensity, it was tornadic for the longest time interval, more than 6.5 h. In fact, storm 2 was identifiable on radar for a remarkable 11 h, although it was not particularly strong and may not have had true supercell characteristics during the first 3 h.

Storm 3 was the most prolific CG lightning producer, generating 310 total flashes during a 5.5-h period. Three of the tornadic cells, all single tornado producers, generated no CG lightning at all. The flash rate for storm 3 can be characterized as moderate, but for the other cells, flash rates are rather weak. Small flash rates were also noted in the tornadic cells spawned by Hurricane Danny in 1985 (McCaul 1987), but no quantitative data were available in that earlier study. Almost all the CG flashes from Beryl's tornadic cells were negative in polarity; only 25 of 804 total flashes from those cells were positive.

b. Meteorological conditions

For the Beryl tornado outbreak, surface temperatures and dewpoints in the inflow region located across eastern South Carolina were quite high, with readings of 27° and 22°C, respectively, at KCAE, and 27° and 24°C at nearby McEntire Air National Guard Base (MMT) during the time of the tornadoes. Surface maps of the region during the outbreak consistently show the presence of a weak trough containing a thermal and kine-

TABLE 2. Statistics of echo histories, tornado histories, and CG lightning histories for 13 tornadic storms in TS Beryl on 16–17 Aug 1994. Mvt: movement; Beg: beginning; Neg: flashes transferring negative charge to ground; Pos: flashes transferring positive charge to ground.

	Echo history[a]				Tornadoes[b]				CG lightning[c]			
ID	First tornado	Mvt[d]	Beg[e]	End[e]	No.	Max Intensity	Beg[e]	End[e]	No. neg	No. pos	Beg[e]	End[e]
1	Govan, SC	164 @ 12	1330	1730	2	F2	1509	1702	53	1	1502	1711
2	McEntire, SC	153 @ 09	1345	0045	4	F2	1730	0002	155	5	1734	0001
3	Columbia, SC	161 @ 11	1445	2330	3	F3	1753	2122	304	6	1545	2114
4	Neeses, SC	144 @ 10	1445	2100	8	F3	1620	2100	130	3	1612	2002
5	Hartwell, GA	142 @ 15	1530	1830	1	F1	1739	1739	0	0	—	—
6	Ware Shoals, SC	127 @ 14	1530	2030	1	F0	1940	1940	16	2	1704	1929
7	York, SC	141 @ 12	1715	2315	2	F2	2150	2245	49	0	1811	2130
8	Earl, NC	140 @ 10	1715	2345	1	F1	2230	2230	26	1	1853	2010
9	Lexington, GA	140 @ 16	1715	1845	1	F2	1815	1815	0	0	—	—
10	Winnsboro, SC	153 @ 14	1845	0000	3	F2	2144	2320	33	4	1932	2244
11[f]	Cowpens, SC	158 @ 15	2130	2215	1	F1	2156	2202	0	0	—	—
12	Lomax, NC	172 @ 10	2200	0115	1	F0	0015	0015	11	3	2358	0113
13	Hickory, NC	168 @ 11	2300	0045	1	F2	2345	2345	2	0	2323	2329

[a] Source: NOWrad mosaics 1200–0300 UTC 16–17 Aug 1994.
[b] Source: *Storm Data,* Aug 1994 (NCDC 1994).
[c] Source: National Lightning Detection Network.
[d] Cell motions (°) (m s^{-1}) are 1-h means during mature phase of storm.
[e] All times UTC are on 16–17 Aug 1994; Beg = beginning and End = ending times.
[f] Cell identification and radar history poorly defined.

matic boundary, lying roughly southwest to northeast across central South Carolina. A sample surface analysis from 1500 UTC (Fig. 3) illustrates this feature. Temperatures and dewpoints hovered around 20°–22°C on the northwest side of the boundary, where winds were from the northeast quadrant. On the southeast side, however, temperatures generally exceeded 25°C with very high dewpoints, and the winds were mostly from the southeast quadrant. This pattern, along with the isobar pattern analyzed in Fig. 3, resembles what would be expected if a weak coastal front propagated inland as a warm front, with a weak Piedmont cool wedge (Bell and Bosart 1988) to its west. Because it had warm-frontal characteristics as it moved slowly northwest, this boundary was evidently too diffuse and shallow to appear clearly in the radar imagery.

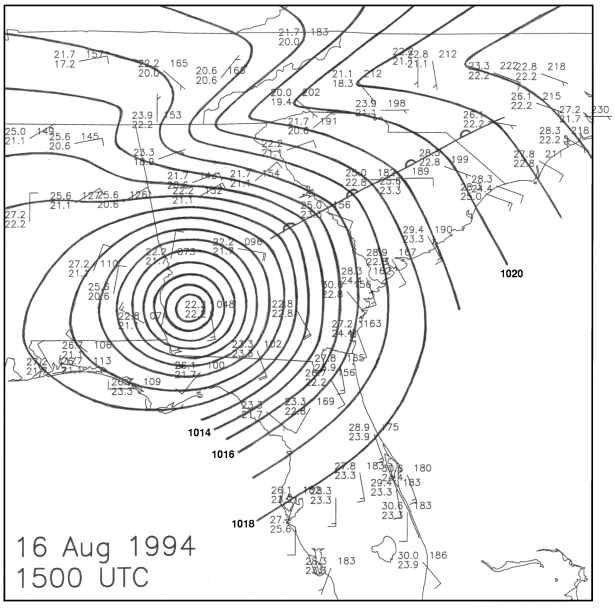

FIG. 3. Regional-scale analysis of surface observations of temperature, dewpoint, sea level pressure, and wind at 1500 UTC 16 Aug 1994, just prior to the onset of the the TS Beryl tornado outbreak. Temperatures and dewpoints are reported in °C, while full wind barbs indicate wind speeds of 5 m s^{-1}. Surface sea level pressures are contoured at 1-hPa intervals to show details of flow over the Carolinas; pressure contours are labeled at selected values, in increments of 2 hPa. Beryl's center is located in southwest Georgia at the time of this analysis.

Unfortunately, the upper-air conditions were not as well defined, inasmuch as no true tornado proximity soundings were available during the most intense phase of the tornadoes in central and northern South Carolina. However, Vescio et al. (1996) examined rawinsonde data from Charleston, South Carolina (CHS), prior to the outbreak, and, noting the surface conditions and the existence of an apparent intrusion of dry air aloft, concluded that early afternoon surface-based convective available potential energy (CAPE) may have been as large as 2000–3000 J kg^{-1}. If correct, these CAPE values are unusually large for a landfalling tropical cyclone environment, according to previous TC tornado proximity sounding climatologies (see, e.g., McCaul 1991). However, in the Hurricane Danny tornado outbreak of 1985. McCaul (1993) found a tornado proximity sounding with CAPE near 2000 J kg^{-1}, based on ascent of parcels representative of the lowest 500 m of the troposphere. Thus, thermodynamic instability conditions diagnosed by Vescio et al. (1996) in the Beryl outbreak appear to have been approximately similar to those found in the 1985 Danny outbreak. One of the numerical

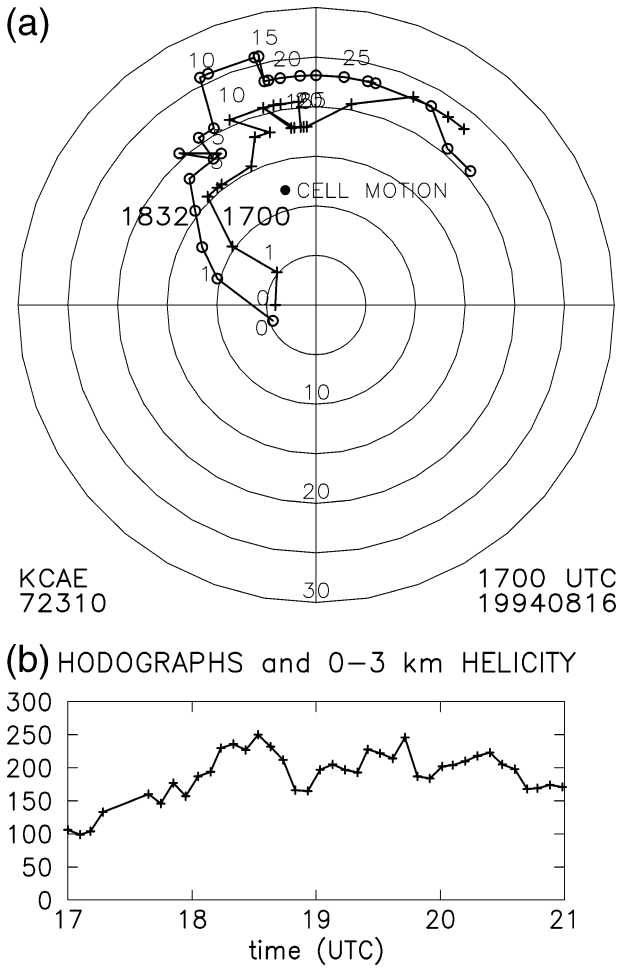

FIG. 4. Wind shear and helicity analysis near the most intense tornadic supercells within TS Beryl on 16 Aug 1994: (a) selected hodographs from WSR-88D-derived wind profiles; rings represent 5 m s^{-1} of wind speed; altitudes are marked in kft at 1, 5, 10, 15, 20, and 25 kft; (b) time series of storm-relative 0–3 km helicity values (m^2 s^{-2}), taken relative to mean storm motion of cells 3 and 4 from Table 2 (blackened circle).

simulations of hurricane-spawned severe convection reported by McCaul and Weisman (1996a) was based on the Danny tornado proximity sounding.

The wind profiles in central South Carolina were inferred from the time series of VAD products at KCAE, as shown in the two selected hodographs in Fig. 4a. In these data, there is likely some reduction of the amplitude of the vertical shear estimates relative to what would have been provided by rawinsonde estimates, owing to the inherent smoothing afforded by the coarse vertical sampling in the radar data (see, e.g., Markowski et al. 1998b). These KCAE VAD data show a period of enhanced vertical shear and 0–3-km storm-relative helicity (H03; Lilly 1986) beginning just before the time the tornadoes were observed southwest of KCAE. The clearest signal of shear enhancement persists for a little more than an hour, from 1739 to 1850 UTC. As seen in the time series in Fig. 4b, H03 values at 1700 UTC, just before the start of this period of shear enhancement, were approximately 100 m^2 s^{-2}, but built up to a peak value of 250 m^2 s^{-2} by 1832 UTC, before starting to decline sharply at 1850 UTC. It is possible that a first peak in H03 occurred during the period when the radar suffered a power outage, between 1722 and 1739 UTC. There is another period of shear enhancement starting at 1900 UTC and culminating at 1943 UTC, when H03 reaches 246 m^2 s^{-2}. A third peak in helicity reaching 223 m^2 s^{-2} occurs at 2024 UTC. Helicity averaged over the lowest 1 km (not shown) also increases in parallel with H03, starting at less than 50 m^2 s^{-2} and rising to more than 120 m^2 s^{-2} by 1832 UTC.

All these shear and helicity values, even if underestimated, are still large enough to suggest likely mesocyclone formation (Davies-Jones et al. 1990) and, for the lowest 1-km shear, the development of tornadoes (Markowski et al. 2002). However, perhaps the most remarkable aspect of the shear and helicity variations in Fig. 4b is the absence of any significant increase in low-level shear at the radar, until the time tornadic storm 4 has approached to within 20 km of the radar site. This and the duration of the period of enhanced helicity culminating at 1832 UTC imply that the zone of strong shear associated with storms 3 and 4 was very narrow. The appearance of two additional peaks in helicity in Fig. 4b shows that there were at least three such zones of enhanced shear in Beryl's right-front quadrant. These variations in shear will be discussed in more detail later.

c. Detailed analyses of supercells

We selected three tornadic storms, those labeled as storms 2, 3, and 4 in Table 2, for detailed radar analysis. These three storms were the most intense and long lived of the 13 tornadic storms in the outbreak. They also passed close enough to KCAE to allow the radar to obtain detailed views of their structure. Figure 5 shows high-resolution low-elevation reflectivity and storm-relative radial velocity fields from KCAE at 1751 UTC over a domain that contains all three storms. The elevation angles shown are those that most clearly describe the essential structure of the storms while minimizing ground clutter interference.

From Fig. 5b, it is apparent that all three storms contain well-defined mesocyclones in the velocity field. Storms 3 and 4 exhibit hook echoes on their southeastern flanks and are producing tornadoes at the time of these radar data. In the velocity field, the rotational couplet, (see the + and − symbols) of storm 3 consists of a tornado vortex signature, in addition to the larger couplet of its parent mesocyclone. Mesocyclone diameters, taken as the distance between the radial velocity extrema, are approximately 2 km, and the storms' heavy precipitation shields are typically about 10 km wide and 20 km long. These dimensions are considerably smaller than those associated with most midlatitude supercell

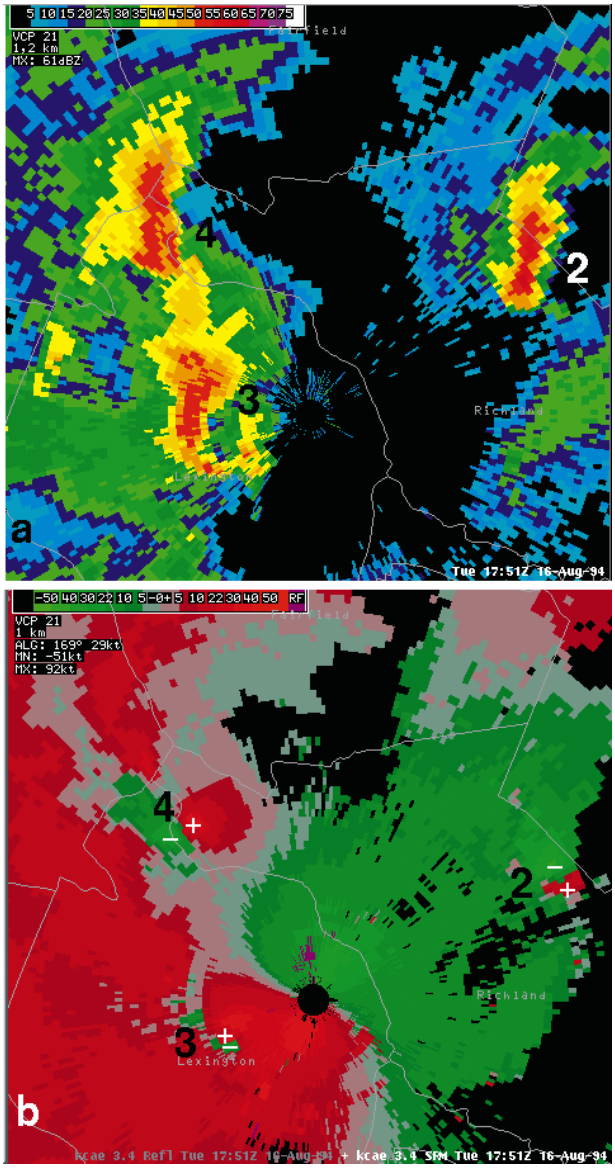

FIG. 5. (a) High-resolution reflectivity and (b) storm-relative radial velocity (kt) fields, at elevation angles 1.5° and 3.4°, respectively, from Columbia WSR-88D (KCAE) at 1751 UTC 16 Aug 1994. Mesocyclones of storms 2, 3, and 4 are labeled for reference in both (a) and (b) and outbound (inbound) velocity maxima are annotated with + (−) symbols in (b). Color contour shades are defined in legend strips at top of (a) and (b). Areas shown are approximately 75 km on each side.

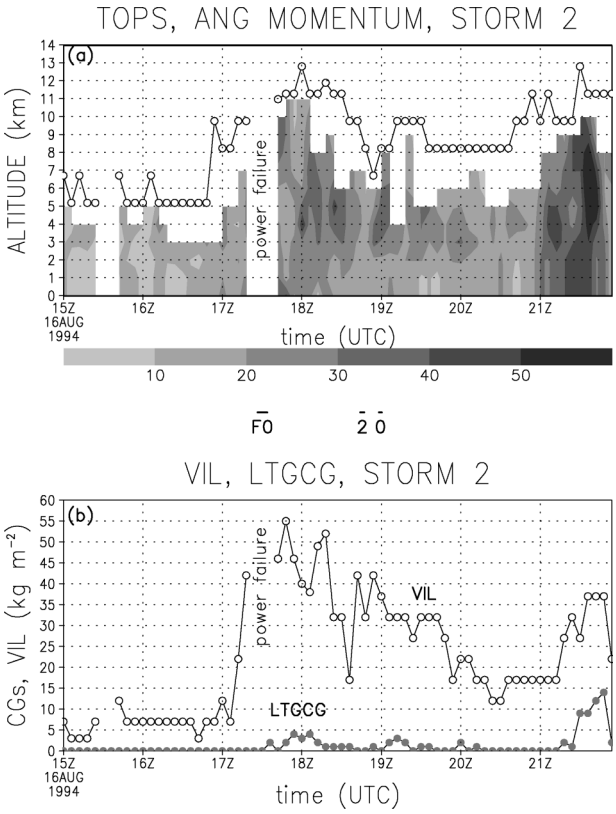

FIG. 6. (a) Radar-derived storm-top height (km) and angular momentum (10^3 m^2 s^{-1}), along with (b) VIL, NLDN CG lightning, and tornado history for tornadic storm 2 (see Table 2). Power failure from 1722 to 1739 UTC was caused by tornado damage from storm 4. CG lightning flashes (LTGCG) per radar volume scan are plotted on same scale as VIL data.

storms occurring on the Great Plains of the United States. Nevertheless, the general characteristics of the tornadic storms in Fig. 5 strongly resemble those described by McCaul and Weisman (1996a) in their numerical study of tropical cyclone–spawned convective storms, especially those occurring in high-CAPE (2000 J kg^{-1}) environments. Those authors concluded that miniature supercell storms could indeed occur in the circulations of landfalling tropical cyclones. It appears that the storms pictured in Fig. 5 are in fact archetypical examples of vigorous tropical cyclone–spawned mini-supercells.

The spatial arrangement of storms 3 and 4 in Fig. 5 is of some interest. Storm 3 followed storm 4's track closely, lagging it by 18 km. The other strong supercell, storm 2, was located some 44 km east of these two storms, and existed in relative isolation. Each of the storms moved generally toward the north-northwest. The existence of a reflectivity bridge between storms 4 and 3 may indicate the presence of an outflow boundary from storm 4 along which storm 3 ''trained.'' However, examination of Doppler velocity data failed to show definitive evidence of a clear velocity signature for such a boundary.

We now turn to a description of each storm's internal structure and evolution. Time–height analyses of radar- and NLDN-derived storm parameters are given in Figs. 6–8, for storms 2–4 respectively. Figures 6a, 7a, and 8a show the contoured field of mesocyclone angular momentum estimated from the radar-observed mesocyclone rotational velocity and core diameter, along with the time series of radar-derived storm-top heights z_T. Angular momentum is depicted instead of rotational

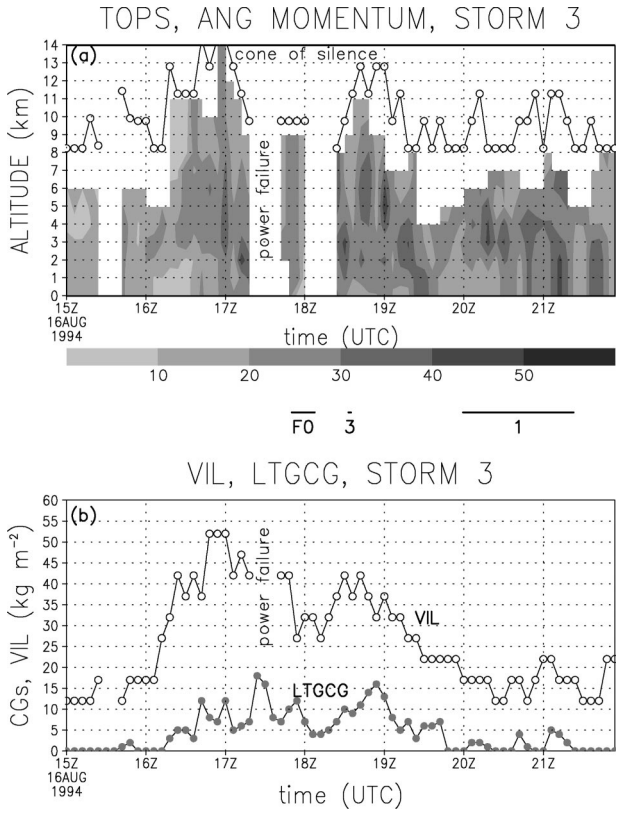

FIG. 7. Radar, NLDN, and tornado history for tornadic storm 3 (see Table 2), plotted as in Fig. 6. Period when storm traversed the radar cone of silence is indicated on plot.

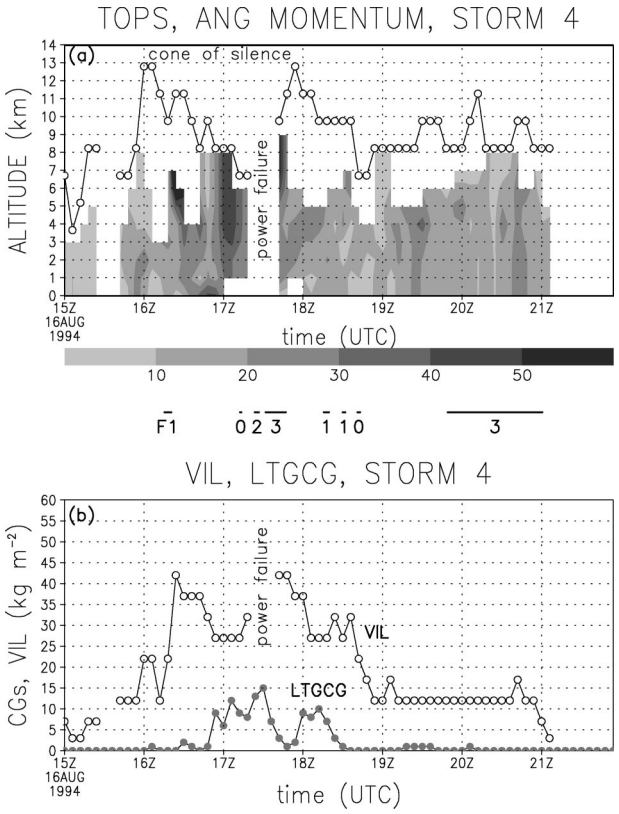

FIG. 8. Radar, NLDN, and tornado history for tornadic storm 4 (see Table 2), plotted as in Figs. 6 and 7. Period when storm traversed the radar cone of silence is indicated on plot.

shear because it tends to be more accurately estimated as range varies, owing to offsetting errors in the radar's measurements of velocity and core diameter. In Figs. 6b, 7b, and 8b, the time series of VIL is furnished along with total CG flashes per radar volume scan. Also shown in these figures are the times and F-scale intensity ratings of the tornadoes produced by each storm.

The three cells studied in Figs. 6–8 exhibit many features in common. Measured values of angular momentum, rotational velocity, and shear were mostly weaker than those found in large midlatitude supercells. For example, rotational shear vorticity values ζ (not shown) were close to 0.02 s^{-1}, but were frequently less than 0.01 s^{-1} at ranges greater than about 80 km from the radar. The largest ζ found was from a tornado vortex signature in storm 4, when it was producing the large and damaging Lexington, South Carolina, F3 tornado; this ζ value peaked at 0.13 s^{-1}. Characteristic rotational velocities V_R were in the 10–15 m s^{-1} range, occasionally reaching the neighborhood of 20–25 m s^{-1}. Mesocyclone diameters (ϕ; not shown) were generally only 2–4 km at close range to KCAE, but showed, as expected, apparent increases as the storms moved farther away from the radar. As a result, peak angular momentum values in the storms tended to lie near 40×10^3 m^2 s^{-1}.

For each storm, typical VIL values were less than 45 kg m^{-2}, although storm 2 produced a brief peak of 55 kg m^{-2}. In several instances, tornadoes are reported even while VIL values are less than 20 kg m^{-2}, especially when the storms are at ranges greater than about 80 km from KCAE. Modal echo-top heights are usually 8–11 km, although occasional pulses to 13–14 km are noted with each storm. Note that in Figs. 7 and 8 storms 3 and 4 both spend more than 1 h in the KCAE cone of silence (see annotations on the figures), at which times their VIL and echo-top data are underestimated. Nevertheless, it is clear from the figures that the typical VIL and echo-top heights found in storms 2–4 are smaller than the typical values found in intense, tornadic Great Plains supercells and are consistent with those found in miniature supercells. The occasional peaks in storm-top height to 13–14 km show, however, that these storms briefly assumed vertical depths approaching those of some midlatitude supercells.

Figures 6–8 show that each of the storms exhibited quasi-cyclic variations in rotation, VIL, and other storm intensity parameters. In storms 3 and 4, tornado reports often tended to occur during periods of increased Doppler-observed mesocyclone rotation, although the intensities of the reported tornadoes are not always proportional to the Doppler-derived vorticity, and the increases

in Doppler rotational velocity are often modest. Considering only tornadoes that occurred when Doppler velocity data are available, all three of storm 3's tornadoes (see Fig. 7) occur during or just after periods exhibiting increases in Doppler-observed rotation. For storm 4 (Fig. 8), six of seven tornado events occur during such periods. For storm 2, which was farther from KCAE than storms 3 and 4, the relationship between tornadoes and Doppler signatures is less clear-cut (Fig. 6). The F2 and F0 tornadoes occurring just before 1900 UTC are not accompanied by obvious increases in low-level Doppler rotational velocity. The first F0 tornado, in progress at 1730 UTC, occurred during the power outage and thus cannot be studied definitively. However, it appears that this tornado was associated with a maximum in Doppler rotational velocity, because rotation was increasing just before the outage, and decreasing at its conclusion.

Despite the tendency for tornadoes to occur during periods of increased mesocyclone rotation, there are many instances of Doppler-observed rotation increase that are not accompanied by reports of tornadoes. Storm 2 features 10 such events, while storm 3 has 7 and storm 4 has 5. Several of these false alarms are quite significant: Storm 2 fails to produce any documented tornadoes near 1800 UTC or, especially, near 2130 UTC, when Doppler indications appear ominous; storm 3 fails to produce tornadoes at 1700–1715 UTC, at 1925 UTC, and again at 2145 UTC; storm 4 fails to produce tornadoes at 1555 UTC, at 1650 UTC, and at 1925 UTC. The widely recognized tendency for the Doppler data to ''overpredict'' tornadoes is apparent in these Beryl radar observations.

The mesocyclones in storms 2–4 were surprisingly well developed in the vertical, compared to other minisupercell storms (see, e.g., Knupp et al. 1998). Vorticity greater than 0.02 s^{-1} was often detected as high as 6-km altitude, and occasionally up to 10 km, during periods of maximum intensity and closest proximity to KCAE. As is commonly observed in other supercells, low-level rotation was often associated with intense convergence, and upper-level rotation with strong divergence. In the raw rotational velocity data (not shown), there are hints of downward growth of mesocyclone vorticity from midlevels to the surface in some cases, and upward growth of initially surface-based rotation in others. These changes are often rapid, however, and the 5-min time resolution of the radar scans is usually too coarse to permit definitive conclusions to be drawn.

In each storm depicted in Figs. 6–8, variations in VIL tend to correlate well with CG lightning rate changes. We reiterate, however, that the VIL data for storms 3 and 4 during the period 1630–1830 UTC are questionable, owing to the passage of those cells through the KCAE cone of silence (range less than about 35 km), where mid- and upper levels of the storms were undersampled. For each storm, VIL values tended to decrease as range from the radar increased. In Fig. 6, however, the VIL of storm 2 displays an increase after about 2110 UTC, but without reaching values seen during 1715–1825 UTC. In contrast, the NLDN CG data reach their maximum rates in this storm after 2110 UTC. This suggests that the tendency for VIL to decrease with range may be a result of the radar's undersampling of the minisupercell storm volume, especially at low levels, as the storms recede from the radar. A similar observation applies to radar-derived estimates of V_R and ζ at long range from the radar, although angular momentum is less affected because of the radar's tendency to compensate any underestimation of V_R by overestimation of ϕ. These undersampling problems become particularly noticeable when the minisupercells move beyond approximately 100-km range from the radar.

In Figs. 6–8, it is seen that the three strongest minisupercells exhibited weak to moderate CG flash rates. Nevertheless, there are instances where CG rates declined during tornado events, after having increased earlier. The first F3 tornado from storm 4, for example, is accompanied by a drop in CG rates to near 0 at 1750 UTC. At the same time, this storm's VIL actually increases slightly. In Great Plains tornadic supercells, well-defined decreases in CG lightning flash rate during tornadogenesis have also been observed (see, e.g., MacGorman and Burgess 1994).

The full temporal histories of CG lightning activity from all 13 tornadic cells are depicted in Fig. 9. Times of reported tornadoes are also indicated on the figure. From this figure, it is clear that storms 2, 3, and 4 were much more prolific CG lightning producers than the other storms. An unexpected yet interesting finding is that many of the weaker storms (see, e.g., storms 6, 7, 8, and 13) tended to produce their tornadoes following cessation of all their CG lightning. The final tornadoes from prolific storms 2, 4, and 10 also seem to occur after final bursts of CG activity, although some of the bursts are only rather weak. These features may be yet another manifestation of the process producing CG lulls seen during tornadoes in some plains supercells (MacGorman and Burgess 1994), except for the additional feature here involving the failure of CG flash activity to resume following the tornadoes.

In an attempt to quantify our impressions of the relationship between CG rates and tornadoes, we computed and compared the average CG flash rates for periods ''before'' and ''during'' the tornadoes in Fig. 9. From inspection of the data, it was apparent that many of the bursts of CG activity within individual storm cells tended to have a time duration of roughly 30 min. Most of the tornadoes tended to be briefer than this; the two long-duration tornadoes associated with storms 3 and 4 were reported by *Storm Data* (NCDC 1994) to have been not in continuous contact with the ground and were likely a series of brief tornadoes. Thus, we examined average CG rates for 30-min periods prior to the start of tornadoes and compared them with the corresponding rates averaged during the lifetimes of the tornadoes, but

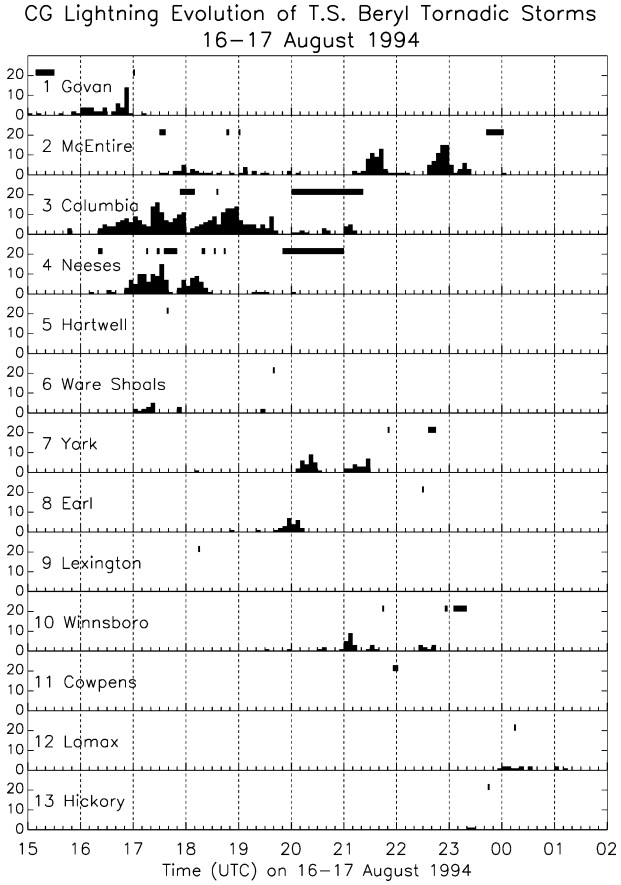

FIG. 9. Histories of CG lightning rate (vertical bars) and tornado occurrences (horizontal bars) for all 13 tornado-producing cells in TS Beryl examined in this study.

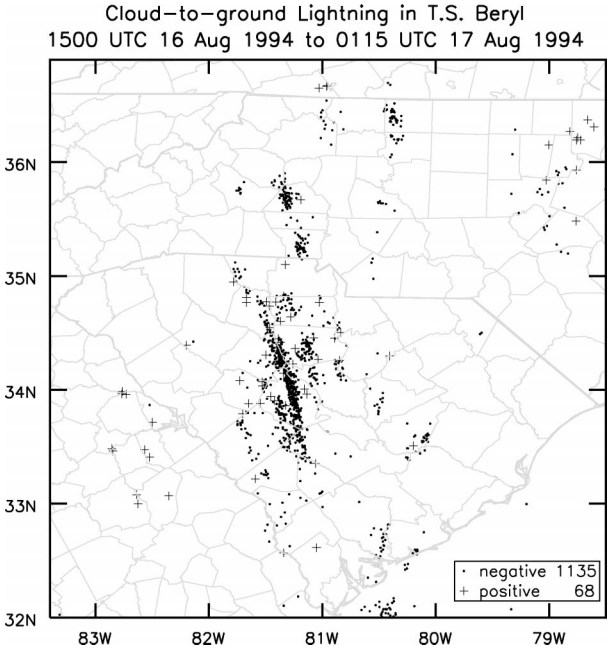

FIG. 10. Map of all CG lightning occurrences within TS Beryl on 16–17 Aug 1994, throughout the region examined in this study. Dots indicate negative ground flashes, while + signs indicate positive flashes. Total flash counts for each polarity are shown at lower right.

with the stipulation that a full 5-min period be used for very brief tornadoes and that the lifetime of the tornado not be allowed to exceed 30 min. The result is that 18 tornadoes had smaller CG rates ''during'' their lifetimes than ''before,'' while only 5 tornadoes had larger CG rates ''during'' than ''before.'' Four other tornadoes had zero CG rates both ''before'' and ''during'' the tornadoes. Application of a sign test (see, e.g., Conover 1980) to these results indicates that there is 99% confidence that the mean ''before'' and ''during'' rates do indeed differ. Furthermore, the mean CG flash rate for the ''before'' period for all tornadoes was 0.54 min^{-1}, more than twice as large as that for the ''during'' period, which was only 0.25 min^{-1}.

The sense of these ''before'' versus ''during'' findings did not change even if the length of the ''before'' period was reduced to 20 or even 10 min, although the statistics were most compelling when 30-min-long ''before'' periods were considered. This is the same duration chosen by Perez et al. (1997) in characterizing CG flash rates ''before'' their sample of violent tornadoes. Our results thus indicate that there is a quantifiable tendency for CG flash rates to be reduced during the tornadoes of this outbreak, compared to 30-min periods prior to the tornadoes. The possible physical significance of this finding, and limitations on its potential utility for tornado nowcasting, are discussed in section 4.

The dominance of storms 2–4 in the CG lightning productivity of Beryl's tornadic storms is obvious in Fig. 9. This does not, however, rule out the possibility that some of Beryl's nontornadic storms might have been as prolific at producing CGs as tornadic storms 2–4. To see if this actually happened, we constructed a map of all CG flashes observed by NLDN during the period 1500 UTC 16 August–0115 UTC 17 August (Fig. 10). This map shows strong clustering of flashes along the tracks of tornadic storms 2–4 (see Fig. 1). The flashes in these cluster streaks were in fact largely produced by the tornadic storms, and not by other storms that happened to have nearly similar tracks. No other comparably dense clustering of flashes is apparent in Fig. 10, which shows that none of the nontornadic storms produced as much CG lightning as tornadic storms 2–4. In fact, of the 1203 total CG flashes shown in Fig. 10, some 804 (66.8%) were produced by the tornadic storms. This concentration of CG activity in the most intense tornadic storms is consistent with impressions gleaned from other lightning studies of tornadic storms in landfalling tropical cyclones in Florida (Sharp et al. 1997).

Although Beryl's tornadic storms generated most of the CG lightning shown in Fig. 10, they did not generate CG flashes with peak currents as strong as the nontornadic storms. Table 3 shows the characteristics of the

TABLE 3. Statistics of CG lightning flashes in TS Beryl tornado outbreak, 1500 UTC 16 Aug–0015 UTC 17 Aug 1994. The following abbreviations are used to describe the various CG lightning flash classes: Neg: flashes transferring negative charge to ground; Pos: flashes transferring positive charge to ground; Num: number of flashes within a class; Med: median peak current (kA); Avg: average peak current (kA); Max: maximum peak current (kA); Min: minimum peak current (kA); Str: strokes per flash; Tor: subset of known tornadic storms; Non: nontornadic storms.

Cell ID	Neg Num	Pos Num	% Pos	Neg Med	Neg Avg	Neg Max	Neg Min	Neg Str	Pos Med	Pos Avg	Pos Max	Pos Min	Pos Str
1	53	1	1.9	−23.1	−24.8	−59.2	−11.3	2.64	10.6	10.6	10.6	10.6	1.00
2	155	5	3.1	−15.2	−16.5	−57.8	−8.9	1.50	14.1	19.8	44.2	11.6	1.00
3	304	6	1.9	−16.5	−18.5	−52.3	−8.2	2.51	17.2	22.6	60.2	9.9	1.17
4	130	3	2.3	−17.3	−20.1	−88.5	−8.7	2.21	14.8	17.4	23.6	13.9	1.67
5	0	0	0.0	0.0	0.0	0.0	0.0	0.00	0.0	0.0	0.0	0.0	0.00
6	16	2	11.1	−16.4	−20.2	−35.8	−12.4	1.56	69.1	41.4	69.1	13.6	1.00
7	49	0	0.0	−15.8	−16.4	−34.9	−9.5	2.06	0.0	0.0	0.0	0.0	0.00
8	26	1	3.7	−13.7	−16.6	−32.9	−11.0	1.73	19.3	19.3	19.3	19.3	1.00
9	0	0	0.0	0.0	0.0	0.0	0.0	0.00	0.0	0.0	0.0	0.0	0.00
10	33	4	10.8	−16.1	−16.8	−24.3	−11.3	2.12	37.6	32.4	55.0	13.1	1.25
11	0	0	0.0	0.0	0.0	0.0	0.0	0.00	0.0	0.0	0.0	0.0	0.00
12	11	3	21.4	−15.2	−17.3	−33.4	−10.8	1.27	43.5	43.5	51.0	36.1	1.67
13	2	0	0.0	−10.1	−14.3	−18.5	−10.1	1.00	0.0	0.0	0.0	0.0	0.00
Tor	779	25	3.1	−16.3	−18.5	−88.5	−8.2	2.16	17.2	26.4	69.1	9.9	1.24
Non	356	43	10.8	−19.8	−24.5	−110.3	−9.0	2.05	23.4	29.8	114.8	9.4	1.09

CG flashes for each tornadic storm, as well as for the classes of tornadic and nontornadic convection in Beryl's remnants. For both positive and negative flash polarities, it is found that the extreme, median, and mean peak current amplitudes are significantly larger for the nontornadic storms. The nontornadic storms also produce a proportion of positive CGs (10.8%) that is more than 3 times that of the tornadic storms (3.1%). Inspection of the map in Fig. 10 reveals that much of the surplus of positive flashes in the nontornadic convection occurs in Georgia, near the core of Beryl's remnants, where all CG flashes were positive. Examination of the peak currents in these core flashes confirms (not shown) that they also tend to contribute to the enhancement of peak current statistics in the nontornadic storms. According to Fig. 10, a separate area of storms in eastern North Carolina (near latitude 36°N, longitude 79°W) also featured a large proportion of positive CGs; these also contained enhanced peak currents but are too far away from Beryl's circulation to be considered in detail here.

Based on the radar data, the core region of TS Beryl in Georgia appeared to be dominated by stratiform precipitation, with embedded convection. Other studies (e.g., Rutledge et al. 1990) have documented the occurrence of positive CG flashes in stratiform rain areas adjacent to convection. Note that while tornadic storms 5 and 9 occurred in Georgia (see Fig. 1), they failed to generate any CG flashes (see Table 2) and do not contribute to the positive flash regime there. With respect to CG stroke multiplicity, Table 3 also shows that there was little difference between tornadic and nontornadic storms; both produced roughly one stroke per positive and two strokes per negative CG.

4. Discussion

The Beryl data represent a good example of intense minisupercell storms in landfalling tropical cyclones, as documented by McCaul (1987) and McCaul and Weisman (1996a). Beryl's minisupercells were quite intense, with mesocyclone signatures sometimes occupying most of the echo depth. Mesocyclone diameters, however, were typically 2–4 km, which is small compared to most Great Plains supercell mesocyclones, but larger than the rotation cores associated with Colorado gust front tornadoes (Wilson 1986). Thus, at least for the tornadoes in Beryl's storms 2–4, the predominant mode of tornado occurrence appears to have been that associated with true minisupercell mesocyclone processes and not nonsupercell gust front processes.

Based on the number and intensity of tornadoes they produced, Beryl's supercells are probably near the top of the spectrum of TC-spawned convective cell intensity. They may, however, not be at the top of the spectrum for TC-spawned supercell size: Sharp et al. (1997) documented supercells over the Gulf of Mexico in 1995's Hurricane Opal with storm tops that rival those found on the Great Plains.

One of Beryl's minisupercells produced tornadoes for as long as 6.5 h and had a total cell lifetime as long as 11 h. Such extreme cell longevity is much larger than had been suspected for TC convective cells, which have been found to possess cell lifetimes over the ocean generally shorter than 35 min (Parrish et al. 1984). The 11-h lifetime of storm 2 is considerably longer than that estimated for the supercells in Hurricane Danny of 1985 (McCaul 1987) and is comparable to the longest ever documented in major midlatitude tornadic supercell events (see Knupp et al. 1996). Because storm 2 was visible on radar for at least a continuous 3-h period prior

to assuming obvious supercell characteristics, we recommend forecasters pay special attention to any long-lasting TC convective cell occurring in a favorable environment, even if the cell appears relatively weak on radar.

The KCAE VAD profiles indicate that storms 2–4 occurred during an approximately 1.0-h-long period of backed surface winds, enhanced vertical shear, and 0–3-km helicity in Beryl's right-front quadrant. Localized enhancements of vertical shear have also been detected in other landfalling TCs (see McCaul et al. 1993; Spratt et al. 1997). Assuming Beryl's zone of enhanced shear propagated at the same speed as its parent cyclone, then its along-TC-track dimension likely did not exceed 40–50 km, a size so small that it is unlikely to be detected by standard rawinsonde measurements. The full shape and size of the zone of enhanced shear remain unknown, however. According to KCAE radar data obtained between 1700 and 2100 UTC, Beryl contained three such zones of enhanced shear, as reflected in 0–3-km helicity variations (Fig. 4). In Beryl's case, the helicity maxima were typically located near the leading edge of heavy convective cells within rainbands. Other TCs have also been found to contain multiple such zones, also associated with major rainbands (see McCaul et al. 1993). The latter paper also shows that zones of enhanced boundary layer virtual temperature, and probably enhanced CAPE, also accompanied the zones of enhanced shear. The enhancements in virtual temperature and CAPE were concentrated just ahead of the rainband wind shift lines and were largest along the outermost rainbands. In Beryl, surface temperatures and dewpoints were highest in eastern South Carolina, northeast of a convective band associated with the first shear maximum that occurred at KCAE at 1832 UTC (see Fig. 4). It is within this region of high dewpoints and increasing shears that storms 2–4 formed.

One interpretation of the association between the supercells and the zones of enhanced shear is that the enhanced shear, and possibly also enhanced CAPE, helped cause the supercells, or at least boost their intensity. Nonetheless, the apparent compactness of the zones of enhanced shear suggests an alternate interpretation, namely that the circulations of the supercells themselves helped cause the enhanced shear (Weisman et al. 1998). After all, even the minima in helicity in Fig. 4 imply shears that are likely capable of supporting storms with rotating updrafts. However, the validity of this latter kind of interpretation appears questionable when the data are examined in detail. Storms 4 and 3 passed just west of KCAE, making their closest approaches to KCAE at around 1715 and 1800 UTC, respectively. The simulations of Weisman et al. (1998) show that the perturbations associated with supercell storms are stronger close to the storms than farther away. Based on their findings, one would expect to see two strong shear peaks, near the times of closest approach of the two storms to KCAE. This is not observed. Instead, the data in Fig. 4 show that the shears continue to increase until about 1830 UTC, some 30 min after storm 3 passes KCAE, when one of Beryl's rainbands approaches KCAE. These findings suggest that it was the larger-than-storm-scale flow structure of the approaching rainband that generated the zone of enhanced shear and helicity in which storms 3 and 4 were embedded. This convective band can be seen in the 1800 UTC panel of Fig. 2; it lies west through south of Columbia, and contains tornadic storm cell 6 near its northwestern end.

While the rainbands of Beryl were important in modulating the vertical shear and helicity in South Carolina during this tornado outbreak, another significant feature enhancing the severe weather potential was the weak warm coastal frontlike boundary that moved slowly northwestward through the central part of the state on 16 August (see Fig. 3 for the 1500 UTC analysis). Figure 1 shows that, although many of the tornadic storms originated in southern South Carolina, the majority of the tornadoes—and all the large ones—occurred in central or upstate parts of the state. Thus it appears that most of the tornadoes occurred near, or a short distance northwest of, this frontal boundary, in slightly cooler surface air with backed surface winds. This preferred location for the tornadoes—just on the cool side of a preexisting boundary—is similar to what has been reported in studies of Great Plains tornado events (Markowski et al. 1998a; Rasmussen et al. 2000).

In summary, the picture that emerges regarding the mesoscale structure of the atmosphere in the vicinity of the Beryl tornadoes involves the interaction of two major features: the series of TC rainbands that moved across South Carolina from the southwest, and the preexisting weak warm coastal frontal boundary over which those rainbands moved. The rainbands provided substantial modulation of the shear and, perhaps, also CAPE. As these small-scale regions of favorable conditions impinged on the warm frontal zone, low-level shears became even more favorable, and the storms, already supercellular in character, generated families of tornadoes, some strong. Storms 2–4 formed in one of these regions of increased shear just ahead of what appears to be the outermost of Beryl's organized rainbands, and produced numerous tornadoes as they moved across the diffuse frontal zone.

Although most of Beryl's CG lightning activity on 16 August was confined to the tornadic cells, the CG flash rates for these cells were not very large. However, the variations in CG flash rates, particularly the decreases during tornadoes, are sufficiently common that they deserve further consideration. Perez et al. (1997) noted that increases in CG rates prior to tornadogenesis may be the result of pulses of updrafts that act to enhance vortex stretching at low levels. However, a candidate mechanism that could actually suppress flash rates during tornadoes, particularly at lower and middle altitudes where the charge layers that trigger most CGs

probably exist, is the so-called vortex-valve effect, which mandates a weakening of low- and midlevel updraft—and probably also charge separation processes—when vorticity maximizes near the surface. Such effects would be most noticeable in storms having a single main updraft that is associated with the tornado. It is possible that this effect could be at least partially responsible for the observed decreases in CG flash rates seen in many of Beryl's storms during their tornadoes.

The pattern seen in CG rate variations in this study—decreased CG rates during tornadoes, relative to the 30-min period prior to the tornadoes—is reminiscent of the findings of Perez et al. (1997) and Kane (1991), although the emphasis in those investigations was on the timing of peak CG rates with respect to severe weather events. Perez et al. (1997) found more than 75% of their violent tornado cases had CG rate minima within 10 min of tornado touchdown, but they caution that peak CG rates in storms occur almost as often after violent tornadoes as before. Indeed, the averaged patterns detected here do not occur consistently in all of Beryl's tornadoes and do not always work for the most intense tornadoes. For example, the F3 tornado in storm 3 occurs during a brief, minor decline in CG rates, embedded in an otherwise increasing CG flash rate trend. The first F3 tornado from storm 4 is characterized by a sharp decline in CG rates, but those rates also reach a storm-lifetime peak in the 5-min period immediately prior to the tornado's touchdown time. Furthermore, there are a number of instances of declines in CG rates in Fig. 9 that are not accompanied by tornadoes. In addition, it is not clear whether the trends seen in the Beryl case will be found in other TC tornado outbreaks. Until further research is done on these types of outbreaks, we urge caution in any attempts to apply our CG flash rate findings to real-world forecasting and warning tasks. Exclusive use of CG rates and trends to identify imminent tornadogenesis is known to be fraught with difficulties, because decreases in CG activity may result from many processes, including actual storm dissipation.

In addition, the Beryl findings suggest that caution is needed in interpreting other more subtle aspects of the CG lightning in landfalling tropical cyclones. For instance, while the tornadic storm cells tend to produce more frequent CG lightning than the weaker nontornadic cells, they do not appear to produce peak current amplitudes or percentage of positive flashes that are enhanced relative to the nontornadic convection. It is possible, however, that significant information is contained in the intracloud flash rates associated with the landfalling TC convection. While Spratt et al. (1998) did not find a strong relation between total lightning and storm severity in the TS Josephine tornado outbreak in Florida on 7 October 1996, it is possible such relations would be apparent in an outbreak like that of Beryl, which was far more intense. A geostationary satellite–based sensor capable of detecting total lightning flash rates in storms (Buechler et al. 2000) would be highly useful in resolving the ambiguous interpretations of lightning data derived solely from CG flashes in such situations.

The KCAE Doppler data showed increases in mesocyclone rotation for most of the tornadoes from storms 2–4, capturing 10 of 13 events adequately, with a probability of detection (POD) of 0.77. However, the radar also depicted many other episodes of enhanced rotation that failed to produce documented tornadoes, with some 22 of 35 total opportunities falling in this category, for a false alarm ratio (FAR) of 0.63. These statistics are roughly consistent with other general experience regarding the capability of the Doppler radars to detect storms with a severe weather threat, showing considerable potential, but with significant limitations as well. At present, it is not clear whether our findings regarding the relationships between Beryl's tornadoes and their radar and CG lighting signatures will be confirmed in other severe TC tornado outbreaks. Much more research remains to be done before firm recommendations can be made about optimal joint use of the radar and CG lightning data in landfalling TC tornado events.

The Beryl tornado event was an excellent example of a tropical cyclone whose biggest danger to the public is from tornadoes. Unfortunately, our ability to anticipate which landfalling TCs will spawn large tornado outbreaks is not well developed. Based on review of data from the Beryl outbreak and from other recent significant TC tornado outbreaks, we have come to suspect that most severe TC tornado outbreaks occur in conjunction with tornado family–producing minisupercell storms. It should be noted that only five supercells, each spawning five tornadoes, can suffice to produce a severe TC tornado outbreak, according to the definition of McCaul (1991). If the average spacing between supercells arranged in a line is roughly 20 km, as found in this and prior studies, then all that is needed to permit the development of a severe TC tornado outbreak is an envelope of favorable conditions only about 100 km long, experiencing an ongoing supply of adequate CAPE for several hours as a result of its propagation and immersion in a suitably sheared environment.

The conditions that support supercell storms are now relatively well known, even for low-CAPE TC environments (see McCaul and Weisman 1996a,b; 2001). Thus it should be possible to forecast which TCs are likely to spawn severe tornado outbreaks, if the spatial distribution of both the buoyancy and vertical shear fields in the landfalling TC can be forecast accurately in advance. This would represent a considerable improvement over current TC tornado forecast capability but would require detailed field observations that describe the evolution of TC kinematic and thermodynamic structure before, during, and after landfall, as well as carefully initialized, fine-resolution mesoscale numerical simulations of the TC. Such improved forecasts of TC tornado outbreak environments might also have implications for evacuation strategies in coastal areas

about to experience a major TC landfall. In 1980, many residents of coastal Texas threatened by powerful Hurricane Allen fled inland to locations that were subsequently raked by Allen's numerous strong tornadoes. The evacuation process, already difficult and frustrating for evacuees, could be improved if reliable forecasts of the location and extent of tornado activity were to become available.

5. Summary and outlook

The TS Beryl outbreak is the most severe TC swarm-tornado event to be studied thus far with the WSR-88D technology. The Doppler radar data collected at KCAE clearly show that many of the tornadoes came from intense minisupercell storms. In a selection of three supercells studied in detail, the reports of tornadoes often corresponded with periods of Doppler-derived increases in mesocyclone rotation, although not very well with peak tornado damage intensity. There were, however, numerous instances in which rotation increased without tornadoes being observed, suggesting a substantial potential for false alarms.

Radar data indicate that these TC minisupercells had modal echo tops of 8–11 km, mesocyclone diameters of 2–4 km, radar-detected rotational velocities of 10–15 m s^{-1}, and vorticities of 0.01–0.02 s^{-1}. Tornado vortex signatures could be detected in mesocyclones within 20 km of the radar, but detection of all mesocyclone features became degraded at ranges beyond 100 km. Perhaps the most remarkable aspect of the tornadic storms was their great longevity; the most persistent tornadic storm was evident in some form on radar for 11 h.

Doppler-derived environmental wind profiles show an approximate 1.0-h period of enhanced shear and helicity during the time when three tornadic supercells passed close to the radar. No finescale data were available to diagnose the thermodynamic structure of this perturbation, which was apparently associated with one of Beryl's outer rainbands, but other circumstantial evidence suggests CAPE was unusually large in the region where the strongest supercells formed. The three strong supercells, and most of the other tornadic storms as well, spawned most of their tornadoes after crossing a diffuse warm coastal front that moved slowly northwest across central South Carolina in advance of Beryl.

NLDN CG lightning activity was examined in detail for this landfalling TC severe swarm-tornado event. Cloud-to-ground lightning rates were largest in the strongest of the tornadic storms, but even for these tornadic storms the rates could only be called weak to moderate. A few of the tornadic cells showed no CG activity at all. Some of the supercells showed decreases in CG activity during tornadogenesis, similar to what has been reported in Great Plains tornadic storms. In several storms, tornadoes occurred after cessation of CG activity altogether. There was a distinct tendency for the CG flash rates to be reduced during tornadoes, compared to the 30-min periods prior to the tornadoes. Unlike the finding for CG flash rates, peak currents in Beryl's CGs were systematically weaker in the tornadic storms than in the nontornadic ones.

Perhaps the biggest remaining gap in our understanding of TC tornado events such as that spawned by Beryl is documentation of variations in CAPE at time and space scales commensurate with the shear profile measurements provided by Doppler radars and profilers. McCaul et al. (1993) found that CAPE was actually largest near the middle of the major rainbands in Hurricane Andrew's remnants, reaching a peak just ahead of the convective wind shift line in each rainband, where anvil rain from the deep convection was also plentiful. At this same location, an along-band low-level jet provided enhanced vertical shear. If this pattern is confirmed in other landfalling TCs, it could suggest that rawinsonde-based climatologies of CAPE within TCs are biased low, because of the difficulty of launching balloons in heavy precipitation. This could explain why mean CAPE values in a previous TC tornado sounding climatology (McCaul 1991) were so small and why there was such a poor correlation between sounding-derived CAPE and tornado outbreak intensity in that study.

More detailed observations of the kinematic structures of weak boundaries, rainbands, and also of the complexities of the TC boundary layer would also be helpful. To address all these issues we recommend regular deployments of instruments such as mobile Doppler radars (Wurman and Winslow 1998), profiles and temperature and water vapor sounders (Knupp et al. 2000), and mobile mesonet stations (Straka et al. 1996) in the outer rainband environments of landfalling TCs, both at landfall and, if possible, for 1–2 days afterward. Such deployments are feasible because the environmental conditions in TC outer rainbands are usually much less dangerous than those within the TC inner core at landfall.

Further studies should also be made with NLDN and also with other ground- or satellite-based sensor technologies that can detect total lightning activity. For optimum impact on forecast capability, these postlandfall measurements must also be closely tied to all available prelandfall data, so that the evolution of TC structural features can be better documented and understood. These new observational capabilities should also be used in conjunction with numerical simulation studies to assess and improve the ability of mesoscale models to describe the fields of thermal instability and vertical shear that promote severe weather occurrences in landfalling TCs.

Acknowledgments. Publication of this paper was supported by NASA Headquarters Earth Science Enterprise through funding from NRA-99-OES-04, ''Investigations that contribute to the NASA Earth Science Enterprise's modeling and data analysis research,'' spon-

sored by Dr. James Dodge, and also by the NWS Eastern Region. The views expressed are those of the authors and do not necessarily represent those of the National Weather Service. Authors EWM and DEB also gratefully acknowledge the assistance of Jason Burks, Tom Bradshaw, John Gordon, Kevin Pence, and their colleagues in the Huntsville and Birmingham NWS offices in reading and interpreting the KCAE radar data. We also appreciate the supportive interest shown by Don Burgess of NSSL. Finally, comments by anonymous reviewers helped improve the content and consistency of the paper substantially.

NOWrad is a registered trademark of WSI Corporation. The NOWrad data and NLDN data were provided by the NASA Lightning Imaging Sensor (LIS) team via the Global Hydrology Resource Center (GHRC), through licensing agreements with WSI Corporation and Global Atmospherics, Inc. (GAI), respectively.

REFERENCES

Bell, G. D., and L. F. Bosart, 1988: Appalachian cold-air damming. *Mon. Wea. Rev.*, **116,** 137–161.

Buechler, D. E., K. T. Driscoll, S. J. Goodman, and H. J. Christian, 2000: Lightning activity within a tornadic thunderstorm observed by the Optical Transient Detector (OTD). *Geophys. Res. Lett.*, **27,** 2253–2256.

Conover, W. J., 1980: *Practical Nonparametric Statistics.* 2d ed. John Wiley and Sons, 493 pp.

Cummins, K. L., M. J. Murphy, E. A. Bardo, W. L. Hiscox, R. B. Pyle, and A. E. Pifer, 1998: A combined TOA/MDF technology upgrade of the U.S. National Lightning Detection Network. *J. Geophys. Res.*, **103,** 9035–9044.

Davies, J., 1990: Midget supercell spawns tornadoes. *Weatherwise,* **43,** 260–261.

——, 1993: Small tornadic supercells in the Central Plains. Preprints, *17th Conf. on Severe Local Storms,* St. Louis, MO, Amer. Meteor. Soc., 305–309.

Davies-Jones, R., D. Burgess, and M. Foster, 1990: Test of helicity as a tornado forecast parameter. Preprints, *16th Conf. on Severe Local Storms,* Kananaskis Park, AB, Canada, Amer. Meteor. Soc., 588–592.

Fujita, T. T., 1981: Tornadoes and downbursts in the context of generalized planetary scales. *J. Atmos. Sci.*, **38,** 1511–1534.

Kane, R. J., 1991: Correlating lightning to severe local storms in the northeastern United States. *Wea. Forecasting,* **6,** 3–12.

Kelly, D. L., J. T. Schaefer, R. P. McNulty, C. A. Doswell III, and R. R. Abbey Jr., 1978: An augmented tornado climatology. *Mon. Wea. Rev.*, **106,** 1172–1183.

Knupp, K., R. L. Clymer, E. McCaul, and K. Pence, 1996: Structure and evolution of the 1994 Palm Sunday tornadic storms and their near mesoscale environment. Preprints, *18th Conf. on Severe Local Storms,* San Francisco, CA, Amer. Meteor. Soc., 42–46.

——, J. Stalker, and E. W. McCaul Jr., 1998: An observational and numerical study of a mini-supercell storm. *Atmos. Res.*, **49,** 35–63.

——, J. Walters, and E. W. McCaul Jr., 2000: Profiler observations of Hurricane Georges during landfall. *Geophys. Res. Lett.*, **27,** 3361–3364.

Lilly, D. K., 1986: The structure, energetics and propagation of rotating convective storms. Part II: Helicity and storm stabilization. *J. Atmos. Sci.*, **43,** 126–140.

MacGorman, D. R., 1993: Lightning in tornadic storms: A review. *The Tornado: Its Structure, Dynamics, Prediction, and Hazards,* C. R. Church, Ed., Amer. Geophys. Union, 173–182.

——, and D. W. Burgess, 1994: Positive cloud-to-ground lightning in tornadic storms and hailstorms. *Mon. Wea. Rev.*, **122,** 1671–1697.

Markowski, P. M., E. N. Rasmussen, and J. M. Straka, 1998a: The occurrence of tornadoes in supercells interacting with boundaries during VORTEX-95. *Wea. Forecasting,* **13,** 852–859.

——, J. M. Straka, and E. N. Rasmussen, 1998b: The sensitivity of storm-relative helicity to small hodograph changes and resolution. Preprints, *19th Conf. on Severe Local Storms,* Minneapolis, MN, Amer. Meteor. Soc., 363–366.

——, C. Hannon, J. Frame, E. Lancaster, and A. Pietrycha, 2002: Characteristics of RUC vertical wind profiles near supercells. Preprints, *21st Conf. on Severe Local Storms,* San Antonio, TX, Amer. Meteor. Soc., 599–602.

McCaul, E. W., Jr., 1987: Observations of the Hurricane ''Danny'' tornado outbreak of 16 August 1985. *Mon. Wea. Rev.*, **115,** 1206–1223.

——, 1991: Buoyancy and shear characteristics of hurricane tornado environments. *Mon. Wea. Rev.*, **119,** 1954–1978.

——, 1993: Observations and simulations of hurricane-spawned tornadic storms. *The Tornado: Its Structure, Dynamics, Prediction, and Hazards,* C. R. Church, Ed., Amer. Geophys. Union, 119–142.

——, and M. L. Weisman, 1996a: Simulations of shallow supercell storms in landfalling hurricane environments. *Mon. Wea. Rev.*, **124,** 408–429.

——, and ——, 1996b: The dependence of simulated storm structure on variations in the shapes of environmental buoyancy and shear profiles. Preprints, *18th Conf. on Severe Local Storms,* San Francisco, CA, Amer. Meteor. Soc., 718–722.

——, and ——, 2001: The sensitivity of simulated supercell structure and intensity to variations in the shapes of environmental buoyancy and shear profiles. *Mon. Wea. Rev.*, **129,** 664–687.

——, K. R. Knupp, and W. L. Snell, 1993: Observations of tornadic storms and rainbands within Hurricane Andrew's remnants. Preprints, *17th Conf. on Severe Local Storms,* St. Louis, MO, Amer. Meteor. Soc., 272–276.

NCDC, 1994: *Storm Data.* Vol. 36, No. 8, 156 pp.

Novlan, D. J., and W. M. Gray, 1974: Hurricane-spawned tornadoes. *Mon. Wea. Rev.*, **102,** 476–488.

Parrish, J. R., R. W. Burpee, F. D. Marks Jr., and C. W. Landsea, 1984: Mesoscale and convective-scale characteristics of Hurricane Frederic during landfall. Preprints, *15th Conf. on Hurricanes and Tropical Meteorology,* Miami, FL, Amer. Meteor. Soc., 415–420.

Perez, A. H., L. J. Wicker, and R. E. Orville, 1997: Characteristics of cloud-to-ground lightning associated with violent tornadoes. *Wea. Forecasting,* **12,** 428–437.

Rasmussen, E. N., S. Richardson, J. M. Straka, P. M. Markowski, and D. O. Blanchard, 2000: The association of significant tornadoes with a baroclinic boundary on 2 June 1995. *Mon. Wea. Rev.*, **128,** 174–191.

Rutledge, S. A., C. Lu, and D. R. MacGorman, 1990: Positive cloud-to-ground lightning in mesoscale convective systems. *J. Atmos. Sci.*, **47,** 2085–2100.

Sharp, D. W., J. Medlin, S. M. Spratt, and S. J. Hodanish, 1997: A spectrum of outer spiral rain band mesocyclones associated with tropical cyclones. Preprints, *22d Conf. on Hurricanes and Tropical Meteorology,* Fort Collins, CO, Amer. Meteor. Soc., 117–118.

Spratt, S. M., D. W. Sharp, P. Welsh, A. Sandrik, F. Alsheimer, and C. Paxton, 1997: A WSR-88D assessment of tropical cyclone outer rainband tornadoes. *Wea. Forecasting,* **12,** 479–501.

——, ——, and S. J. Hodanish, 1998: Observed relationships between total lightning information and Doppler radar data during two recent tropical cyclone tornado events in Florida. Preprints, *19th Conf. on Severe Local Storms,* Minneapolis, MN, Amer. Meteor. Soc., 659–662.

Straka, J. M., E. N. Rasmussen, and S. E. Fredrickson, 1996: A mobile mesonet for finescale meteorological observations. *J. Atmos. Oceanic Technol.*, **13,** 921–936.

Suzuki, O., N. Hiroshi, O. Hisao, and N. Hiroshi, 2000: Tornado-producing mini supercells associated with Typhoon 9019. *Mon. Wea. Rev.*, **128,** 1868–1882.

Vescio, M. D., S. J. Weiss, and F. P. Ostby, 1996: Tornadoes associated with Tropical Storm Beryl. *Natl. Wea. Dig.*, **21,** 2–10.

Weisman, M. L., M. S. Gilmore, and L. J. Wicker, 1998: The impact of convective storms on their local environment: What is an appropriate ambient sounding? Preprints, *19th Conf. on Severe Local Storms*, Minneapolis, MN, Amer. Meteor. Soc., 238–241.

Wilson, J., 1986: Tornadogenesis by nonprecipitation induced wind shear lines. *Mon. Wea. Rev.*, **114,** 270–284.

Wurman, J., and J. Winslow, 1998: Intense sub-kilometer-scale boundary layer rolls observed in Hurricane Fran. *Science*, **280,** 555.